Journal of Alloys and Compounds, 844 (2020) 156092

Effect of pressure on the phase stability and magnetostructural transitions in nickel-rich NiFeGa ribbons

A.F. Manchón-Gordón[1], J.J. Ipus[1], M. Kowalczyk[2], A. Wójcik[3], J.S. Blázquez[1*], C.F. Conde[1], W. Maziarz[3], P. Švec Sr.[4], T. Kulik[2], A. Conde[1]

[1]*Dpto. Física de la Materia Condensada, ICMSE-CSIC, Universidad de Sevilla, P.O. Box 1065, 41080 Sevilla, Spain*
[2]*Faculty of Materials Science and Engineering, Warsaw University of Technology, 141 Wołoska st., 02-507 Warsaw, Poland*
[3] *Institute of Metallurgy and Materials Science, Polish Academy of Sciences, 25 Reymonta Street, 30-059 Kraków, Poland*
[4]*Institute of Physics. Slovak Academy of Sciences. Dúbravská cesta 9, 845 11 Bratislava 45. Slovak Republic.*

[*]*The corresponding author e-mail:* jsebas@us.es

ABSTRACT:

Ribbons of a $Ni_{55}Fe_{19}Ga_{26}$ Heusler alloy were prepared by melt spinning technique. The effect of pressure on magnetostructural transitions was studied comparing as-spun ribbons to ribbons previously submitted to an axial pressure and to powder obtained from manually grinded as-spun ribbons. The martensitic transformation present in the as-spun ribbon almost vanishes after pulverization. The structural change driven by mechanical treatment is a stress-induced intermartensitic transformation from a 14M modulated to a non-modulated tetragonal (NM) structure. There is a progressive change from the structure of as-spun samples to that of the pulverized one in samples submitted to axial pressures as it increases.

KEYWORDS: Magnetic shape memory alloys; martensite structure; 14M modulated phase; magnetostructural transition.

1. INTRODUCTION

Since the discovery of the ferromagnetic shape memory alloys (FSMA) by the groups of Chernenko [1] and Ullako [2], these materials have drawn much attention as potential candidates for many applications [3, 4]. The applicability of FSMA systems is related to

the martensitic transformation (MT), a diffusionless first order phase transition that implies magnetization changes in these alloys.

Several kinds of X_2YZ Heusler alloys exhibit this phase transition. As one of the representative examples, NiMnGa compounds are well-studied systems because of their quite large magnetic-field-induced strain [5]. However, the poor ductility of the alloys of this system limits their applications. Therefore, the development of new systems is needed to overcome this handicap. In this sense, the Ni-Fe-Ga Heusler alloys are highly considered as an alternative to the brittle Ni-Mn-Ga alloys [6]. The improved ductility of these Ni-Fe-Ga alloys has been attributed to the precipitation of the secondary γ phase. Although a low quantity of this secondary phase has benefits on the mechanical properties, a high percentage reduces the transformable phase and hence the shape memory properties.

Stoichiometric Ni_2FeGa composition is located in the β ($L2_1$ or B2) + γ biphasic region of the ternary Ni-Fe-Ga phase diagram [7, 8]. Therefore, the competition between the formation of β and disordered γ phases makes necessary to use rapid quenching techniques, like melt-spinning, in order to produce a single β phase alloy.

Generally, the martensitic transition takes place on cooling between an austenite, with B2 or ordered $L2_1$ structure, and either a modulated (seven-layer, 14M, or five-layer, 10 M) or a non-modulated ($L1_0$ tetragonal) martensite structure, depending on composition and thermal history [9]. However, it has been shown that melt-spinning technique may give rise to a rich variety of micromodulated structures [10], affecting the martensitic transformation.

Although several observations have been made for Ni-Fe-Ga melt-spun ribbons [11-14], pulverized samples (even just manually grinded samples) can exhibit very different structures affecting the martensitic transition and leading to strong impoverishment of

the properties. This effect is also observed in other alloys that loose the martensitic transformation observed in bulk form when they are pulverized [15-17]. This effect is usually ascribed to a severe deformation and atomic disordering of the powder samples after milling [18]. However, in this paper we will show that this is not the case but a non-reversible mechanically induced transition occurs. In order to do so, we studied the effect of applying an axial pressure perpendicular to the plane of the ribbons on the stability of the modulated phase.

2. EXPERIMENTAL

The alloy with nominal composition $Ni_{55}Fe_{19}Ga_{26}$ was prepared in an induction furnace using high-purity elements (>99.9 %). The ingots were melted several times in order to ensure homogeneity. Then, about 30 g of the ingot were induction melted in a quartz tube under argon atmosphere and ejected onto a rotating wheel with a surface velocity about 25 m/s. The thickness and width of the ribbon are about 0.06 and 3 mm, respectively.

The chemical composition of the ribbon was analyzed by X-ray fluorescence using a EAGLE III instrument with an anticatode of Rh.

In order to evaluate the effect of mechanical treatment on the martensitic transformation, pieces of the ribbon occupying a surface of 0.785 cm^2 were pressed with an axial hydrostatic press (loads of 2, 5 and 10 tonnes during 5 min). This treatment did not produce any breaking of the ribbon pieces. Moreover, powder samples were made from the as-spun ribbon by crushing it in an agate mortar.

The starting and finishing temperatures of the martensitic and austenitic transformations were determined by differential scanning calorimetry (DSC) using a Perking-Elmer DSC 7 under Ar flow.

Heat treatments were performed in a differential thermal analysis (DTA) Perkin-Elmer DTA7 unit under Ar flow. Powder samples were heated at 10 K/min up to different temperatures (from 473 K to 1273 K), then annealed at constant temperature for 10 min, and then cooled down to room temperature at 10 K/min.

The microstructural characterization was carried out by X-ray diffraction (XRD) and transmission electron microscopy (TEM). XRD experiments were performed in a Bruker D8 I diffractometer (Cu-Kα, λ=1.5406 Å) and in a Bruker D8 Advance diffractometer (Cr-Kα, λ=2.28970 Å). TEM observations were developed in a Tecnai G2 microscope operating at 200 kV. Thinning of the samples for TEM was carried out in a TenuPol-5 double jet electropolisher using nitric acid and methanol as electrolyte at a temperature of about 250 K.

The local environment of Fe atoms was analyzed at room temperature by Mössbauer spectrometry (MS) in transmission geometry using a ^{57}Co(Rh) source. Values of the hyperfine parameters were obtained by fitting the measured spectra with the NORMOS program [30] and the isomer shift (δ) was quoted relative to that of an α-Fe foil at room temperature. Magnetization measurements were performed in a vibrating sample magnetometer (standard option of a Quantum Design Physical Properties Measurement System, PPMS) applying a magnetic field of 0.01 T.

3. RESULTS and DISCUSSION

The chemical composition of the ribbon has been evaluated from both the free and the wheel side by means of X-Ray fluorescence. Results are summarized in Table 1. There are no significant differences between both sides of the ribbon and the composition agrees with the nominal one. Additionally, the point analyses and elemental mappings show a homogeneous distribution of the elements.

Table 1. Chemical composition measured on both sides of $Ni_{55}Fe_{19}Ga_{26}$ melt-spun ribbon.

Side of ribbon	at. % Ni	at. % Fe	at. % Ga
free side	54.72±0.12	19.20±0.16	26.08±0.21
wheel side	54.41±0.11	19.22±0.15	26.37±0.20

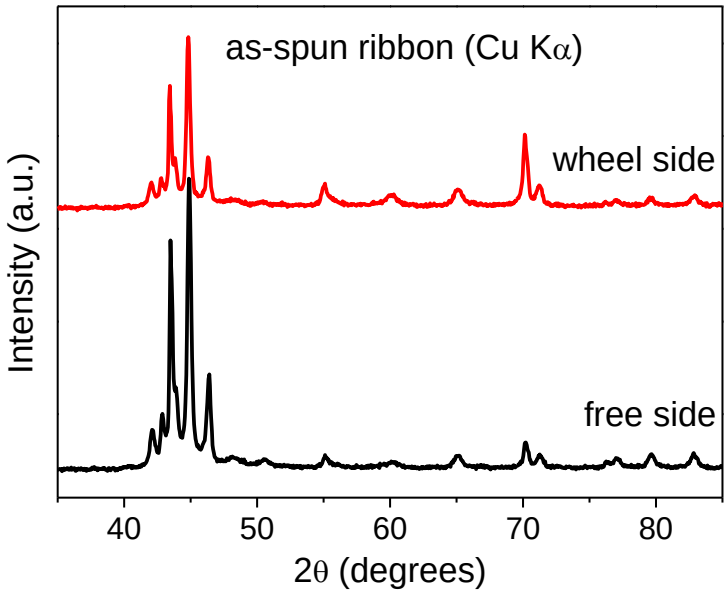

Figure 1. XRD patterns of $Ni_{55}Fe_{19}Ga_{26}$ as-spun ribbon for the wheel (upper) and the free (bottom) sides, respectively, using Cu Kα radiation.

The crystal structure of the as-spun ribbon was identified by X-ray diffraction (XRD) measurements. Figure 1 shows the corresponding XRD patterns taken from both the wheel and the free surfaces of the studied sample. The as-spun ribbon exhibits a modulated type martensite structure in agreement with Ref. [19]. Small differences in the intensities of peaks between both sides of the ribbon can be observed. This could be connected with different size of grains at both sides as a consequence of different cooling rates. TEM observations confirm XRD results. Figure 2 shows a bright field (BF) high magnification image and the corresponding selected area diffraction pattern (SADP) for the as-spun ribbon. SADP can be indexed as seven-layered 14M martensite structure, with six extra spots between two fundamental maxima. This structure for the

martensitic phase has been previously reported for Ni-Fe-Ga alloys with the same composition prepared by arc-melting [20], although not at room temperature.

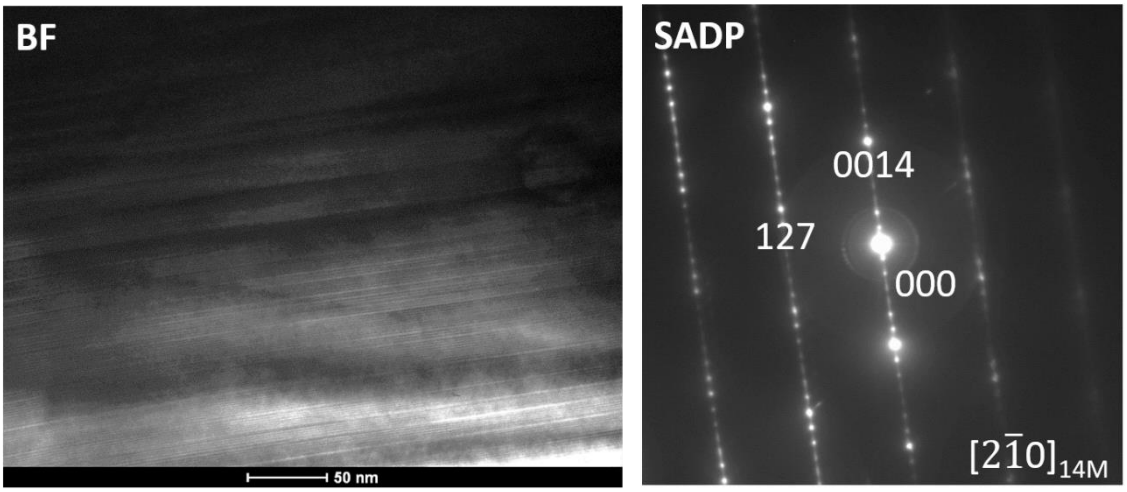

Figure 2. (left) TEM BF image (the white bar corresponds to 50 nm) and (right) corresponding SADP (zone axis is indicated) for the as-spun ribbon.

The thermal behavior of $Ni_{55}Fe_{19}Ga_{26}$ was investigated by differential scanning calorimetry. The DSC curve registered at 20 K/min for the as-spun ribbon is shown in Figure 3 along with those of the ribbon samples heated up to the indicated temperatures at this heating rate. The endothermic and the exothermic peaks in the heating and cooling curves, respectively, clearly indicate the occurrence of a first order phase transition, as expected for martensitic transformations. The austenite start temperature is A_S=395 K for the as-spun ribbon at a heating rate of 20 K/min. This temperature as well as the enthalpy of the transition decrease when the samples are heated above the martensitic transformation (see Table 2). These results are in agreement with those reported by Tolea *et al.* [21], and confirm that subsequent thermal treatments promote a continuous reduction of the MT temperature as well as changes in the transformation heat in Ni-Fe-Ga-(Co) ribbons. However, the latter parameter can be underestimated due to problems associated to the experimental baseline in the range of low temperatures analyzed, close to the limit of measurement range of the DSC. In any case,

the obtained results suggest that the ribbon experiences a structural modification during heat treatments.

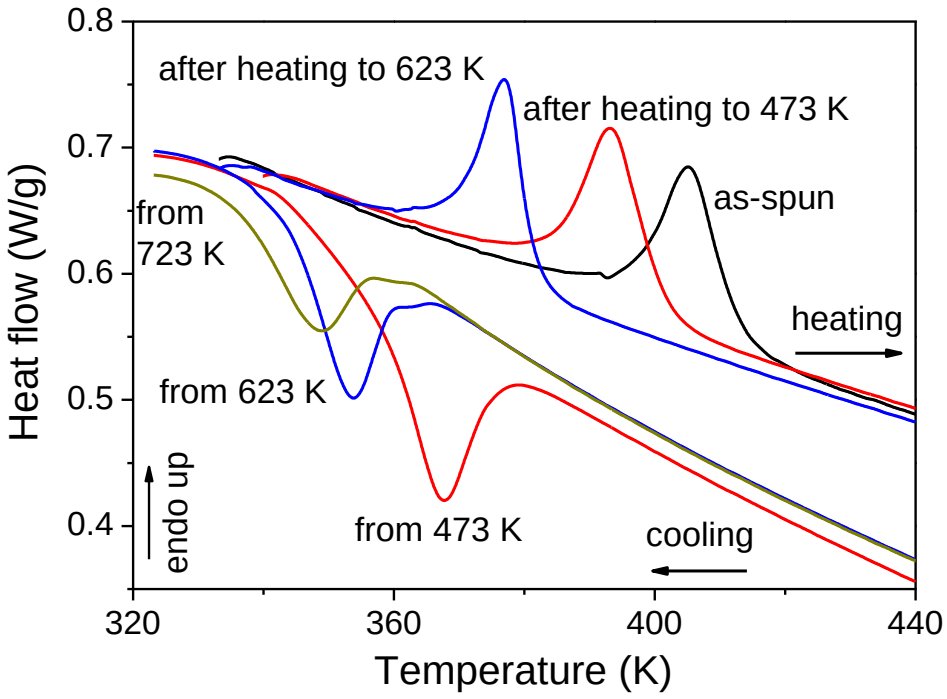

Figure 3. DSC scans at 20 K/min of $Ni_{55}Fe_{19}Ga_{26}$ ribbon showing the shift of the martensitic transformation peak temperature with the indicated previous thermal treatment.

Table 2. DSC parameters of the as-spun ribbon, annealed ribbon samples and powder sample. A_S is the austenite start temperature and H is the entalphy of the martensite to austenite structural transition. The phase fraction of the 14M phase is estimated assuming 100 % of this phase in the as-spun ribbon.

Sample	**A_S (K)**	**H (J/g)**	**14M phase fraction (%)**
As-spun ribbon	395	6.04	100
Ribbon heated up to 473 K	382	5.52	91
Ribbon heated up to 623 K	371	4.83	80
Ribbon heated up to 673 K	367	4.53	75
Ribbon after 2 ton	390	3.00	50
Ribbon after 5 ton	390	1.38	23

Ribbon after 10 ton	388	1.05	17
Powder sample	390	0.3	5

The effect of axial pressure on the structure of the ribbon has been studied. Figure 4 shows the XRD patterns of the as-spun ribbon and after application of load (2, 5 and 10 tonnes) on a 0.785 cm^2 surface during 5 minutes at room temperature, along with that of powder obtained by manually crushing the as-spun ribbon. The increase of the pressure leads to a gradual transformation from the 14M modulated phase to a non-modulated (NM) structure. In the case of the powder pattern, every Bragg peak can be indexed with a tetragonal non-modulated martensitic structure $L1_0$. Stress-induced shift of intermartensitic transformations from modulated to NM phases has also been reported for Ni-Mn-Ga monocrystals [22, 23]. Moreover, ab initio calculations suggest that the NM structure is thermodynamically more stable than the 14M structure [24]. Therefore, both the mechanical stress induced by the pressure and the crushing of ribbon to powder yield relaxation phenomena that help to form the thermodynamically stable NM phase.

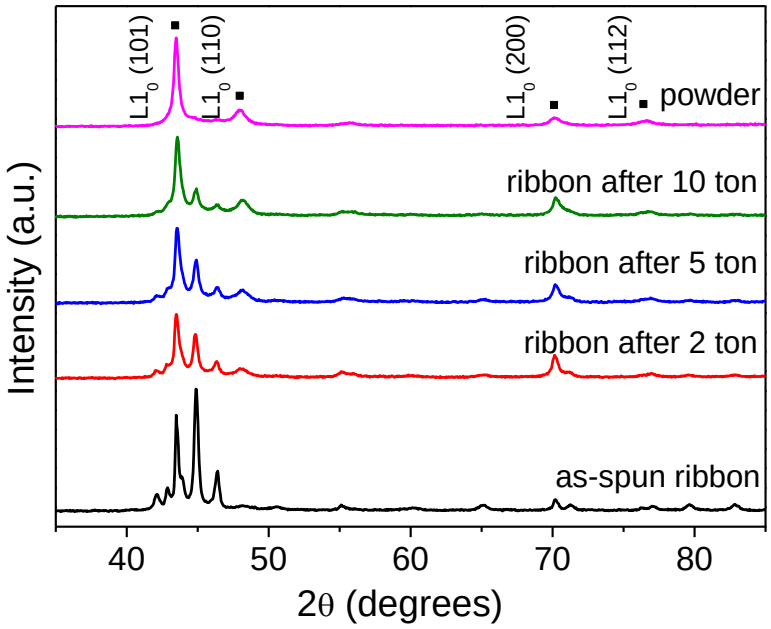

Figure 4. XRD patterns, using Cu Kα radiation, of $Ni_{55}Fe_{19}Ga_{26}$ as-spun ribbon and after applying different mechanical treatments.

DSC scans of mechanically treated samples are shown in Figure 5. The well-defined endothermic peak ascribed to the martensitic transformation observed in the as-spun samples suffers a clear decrease with the mechanical treatment (see Table 2) and, in the pulverized sample, the enthalpy of transformation is reduced in an order of magnitude (curve zoomed x10 in figure 5). Following the XRD results, this suggests that in the studied samples a first-order transition between the martensite and the austenite structures only occurs when the martensite phase exhibits the modulated structure. Therefore, the enthalpy change could be used to estimate the phase fraction of the 14M structure in the samples if a 100% of this structure in the as-spun ribbon is assumed. The results of this analysis is collected in Table 2 along with the values of the austenite transformation start temperatures, A_S, determined by the two-tangent method. Unlike what was observed for thermally treated samples, no clear tendency is observed for A_S with the increase of the applied pressure.

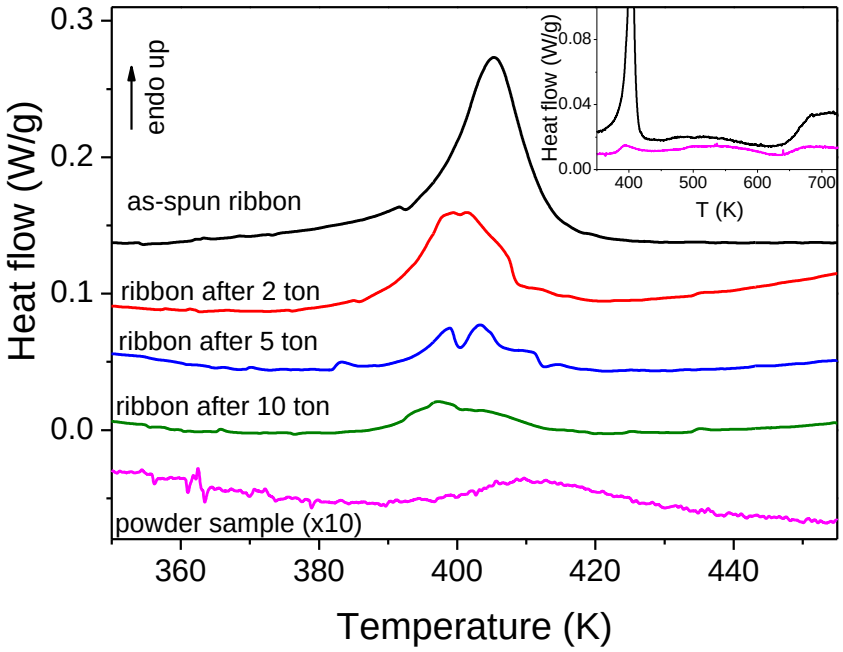

Figure 5. DSC heating scans at 20 K/min of the different studied samples. The plot for the powder sample is zoomed vertically x10. Inset shows DSC scans of the as-spun ribbon and powder in a broader temperature range.

Figure 6 shows the room temperature Mössbauer spectra of the as-spun and mechanically treated samples. A continuous evolution can be inferred from the as-spun ribbon to the powder spectra through the axially pressed ribbons as the applied pressure increases. This is in agreement with the XRD and DSC results, showing the progressive structural change from 14M to NM structure and the reduction in the enthalpy of the transformation peak.

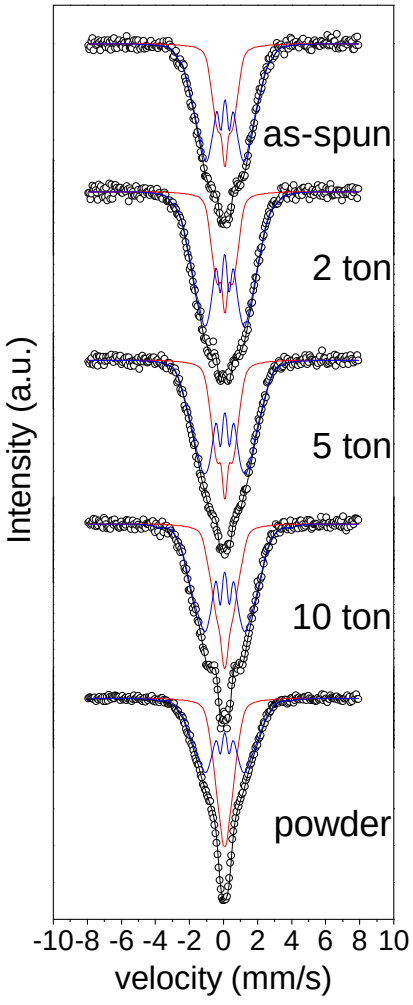

Figure 6. Experimental room temperature Mössbauer spectra (symbols) and model fitting (lines) of $Ni_{55}Fe_{19}Ga_{26}$ as-spun and mechanically treated ribbon and powder samples.

Two components have been used to fit the Mössbauer spectra: a distribution of hyperfine fields (B_{hf}), from 5 to 25 T to describe the ferromagnetic (FM) contributions, and an artificial distribution of hyperfine fields, from 0 to 8 T not ascribed to FM sites but to describe the paramagnetic (PM) contributions. Although a more realistic model should fit the PM contributions using a quadrupolar distribution [25], this leads to strong overlapping and difficulties in the convergence of the fitting. In order to avoid these problems, we have used the area of this low B_{hf} contribution to account for the PM fraction of the studied samples. This procedure is generally found when analyzing strongly disordered systems such as amorphous/nanocrystalline alloys [26, 27]. In our case, the rapid quenching technique and the complex unit cell may have led to the presence of disordering requiring such distributions.

Table 3. Hyperfine parameters obtained from the room temperature Mössbauer spectra of the as-spun and mechanically treated ribbons along with those of powder sample. $<B_{hf}>$ is the main value of the magnetic hyperfine field, δ the isomer shift relative to α-Fe and A the Fe atomic fraction in PM and FM contributions.

Sample	Component	$<B_{hf}>$ (T)	δ (mm/s)	A (%)
As-spun ribbon	PM	3.20	0.064	29.2
	FM	10.12	0.072	70.8
Ribbon after 2 ton	PM	3.47	0.065	27.0
	FM	10.60	0.052	73.0
Ribbon after 5 ton	PM	3.54	0.062	33.1
	FM	10.69	0.063	66.9
Ribbon after 10 ton	PM	3.62	0.057	35.1
	FM	10.97	0.055	64.9
Powder sample	PM	2.89	0.050	43.8
	FM	10.70	0.050	56.2

The hyperfine parameters obtained from the fit of the Mössbauer spectra are summarized in Table 3. From these fits, an increase of the PM contribution with the increase of the applied pressure has been detected and the maximum value corresponds to the powder sample. The measured values range from 29 % to 44 % for the as-spun ribbon and the powder samples, respectively. The results of the as-spun ribbon agree

with those reported by Gutierrez *et al.* [19] for the $Ni_{55}Fe_{19}Ga_{26}$ alloy with 14M. For this sample they found PM contributions even at temperatures well below the martensitic transformation temperature. However, Rama Rao *et. al* [13] reported a totally FM character at room temperature for a $Ni_{2.12}Fe_{0.88}Ga$ with a 10M martensite structure.

To explore whether or not the 14M phase could be recovered by thermal treatments (as it was found for NiMnGa [23]), high temperature annealing experiments were conducted on powder samples annealed as it is described in the experimental section. The crystal structure of the powder samples after these thermal treatments was identified by XRD using Cr Kα radiation. XRD patterns are shown in Figure 7 where that of the as-crushed powder sample has also been included for comparison.

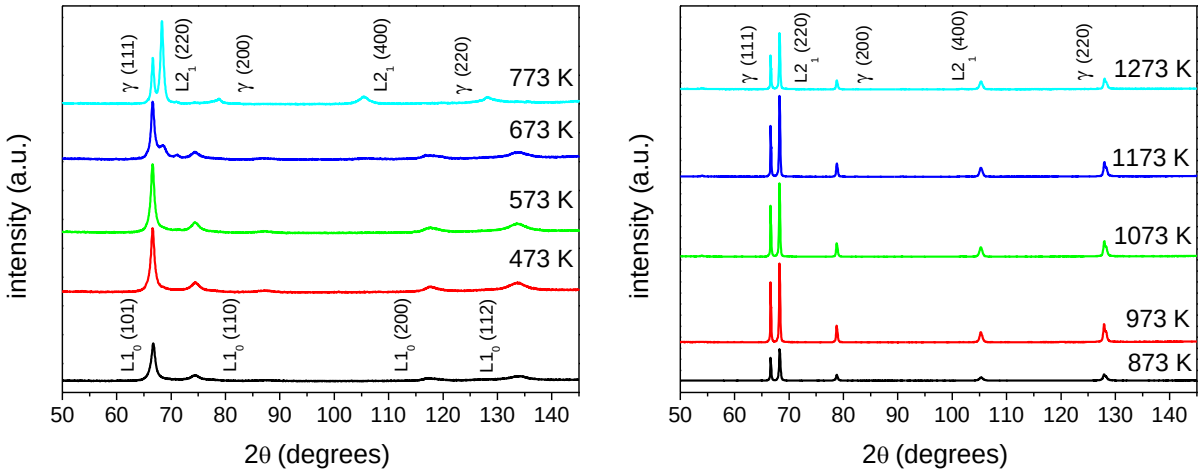

Figure 7. Cr Kα radiation XRD patterns for $Ni_{55}Fe_{19}Ga_{26}$ powders after annealing up to the marked temperatures.

As mentioned above, in the case of the as-crushed powder, a tetragonal NM martensitic structure $L1_0$ is the only phase detected. This structure does not change significantly upon annealing at 473 and 573 K but only a slight change of lattice parameters leading to an increase of c/a ratio can be observed. However, after heating up to 673 K, new

diffraction maxima are detected. Compared to single-phase samples, the peaks of the $L1_0$ phase in this sample shifts to slightly higher angles, probably due to the changes in composition of the martensite as the $L2_1$ phase is developed. Samples treated at temperatures above 673 K exhibit a mixture of two phases that can be indexed as $L2_1$ austenite and γ phases. Small differences in the intensities of the peaks corresponding to $L2_1$ austenite and the γ phases can be observed between the different samples. For samples heated up to 973 K, the intensity of the peaks increases with the increase of temperature, connected with an increase of the crystal size. However, above 973 K, the intensity of some peaks decreases. It is worth noticing that Oikawa *et al.* [28] found that, after heat treatment, the ordered $L2_1$ structure is transformed to the partially ordered B2 structure during quenching, and that the $L2_1$ to B2 order-disorder transition temperature is near 973 K. However, the XRD reflections of this kind of disordered structure coincide with those of the ordered $L2_1$ structure and then they cannot be distinguished if some B2 remnant phase is preserved at room temperature after cooling. Therefore, other techniques, such as TEM or Mössbauer spectroscopy, are necessary in order to clarify the order-disorder transformation results.

Following the XRD results of the powder samples, the principal effect of the thermal treatment is to stabilize the austenite phase at room temperature. This phase transformation from room temperature stable martensite $L1_0$ to room temperature stable austenite $L2_1$ completes only after heating up to a temperature above 673 K. In fact, as it was shown in the inset of Figure 5, the DSC heating scan of the powder sample heated up to 773 K exhibits a broad exothermic peak around 650 K. This should be associated with an irreversible arrangement of the austenite phase that stabilizes it at the room temperature. This peak is present not only in powder samples. In fact, it is also observed in the DSC scans of the as-spun ribbon heated up to 873 K. Room temperature XRD

pattern of the ribbon treated at 873 K also shows the coexistence of the $L2_1$ and γ phases as in the case of the powder sample. This kind of DSC peak has also been reported on heating of as-milled Ni-Mn-In alloys, and was linked to a microstructural recovery process [16]. However, unlike Ni-Mn-Ga [23], in the Ni-Fe-Ga composition studied here, the original modulated structure cannot be recovered, at least, by the thermal procedure of the present study.

Figure 8 shows the room temperature Mössbauer spectra of powder samples annealed for 10 min at the marked temperatures. After heat treatment at 473 K, the spectrum shows a typical single peak characteristic of a sample in PM state, plus a background contribution which indicates the presence of some magnetically ordered phase, in agreement with the spectrum of the as-crushed powder shown in Figure 6. Annealing process leads to a decrease of the disordering found in as-spun ribbons, allowing us to use discrete sites to fit the spectra. The PM contribution has been fitted using two doublets and the FM contribution has been fitted using three different sites with hyperfine fields close to 9, 12 and 16 T. A continuous evolution occurs from samples annealed at 473 K to those annealed at 1273 K. From the fits, the decrease of the PM contributions in the samples is clearly evidenced for samples annealed below 873 K (minimum contribution of both PM doublets, 4%). This is in agreement with XRD results, showing the disappearance of the martensite phase and the emergence of the FM austenite and gamma phases. After annealing above 973 K, the PM contribution can be fitted with a unique doublet. This new PM contribution increases being maximum for the sample treated at 1273 K (63 %), despite structural phase change was not observed in the XRD patterns. Moreover, the hyperfine field of the FM sites used in the fitting shifts to higher values, leading to an increase of the mean value of the hyperfine field,

<B_{hf}>. The resulting fitting hyperfine parameters obtained for the analyzed samples are collected in Table 4.

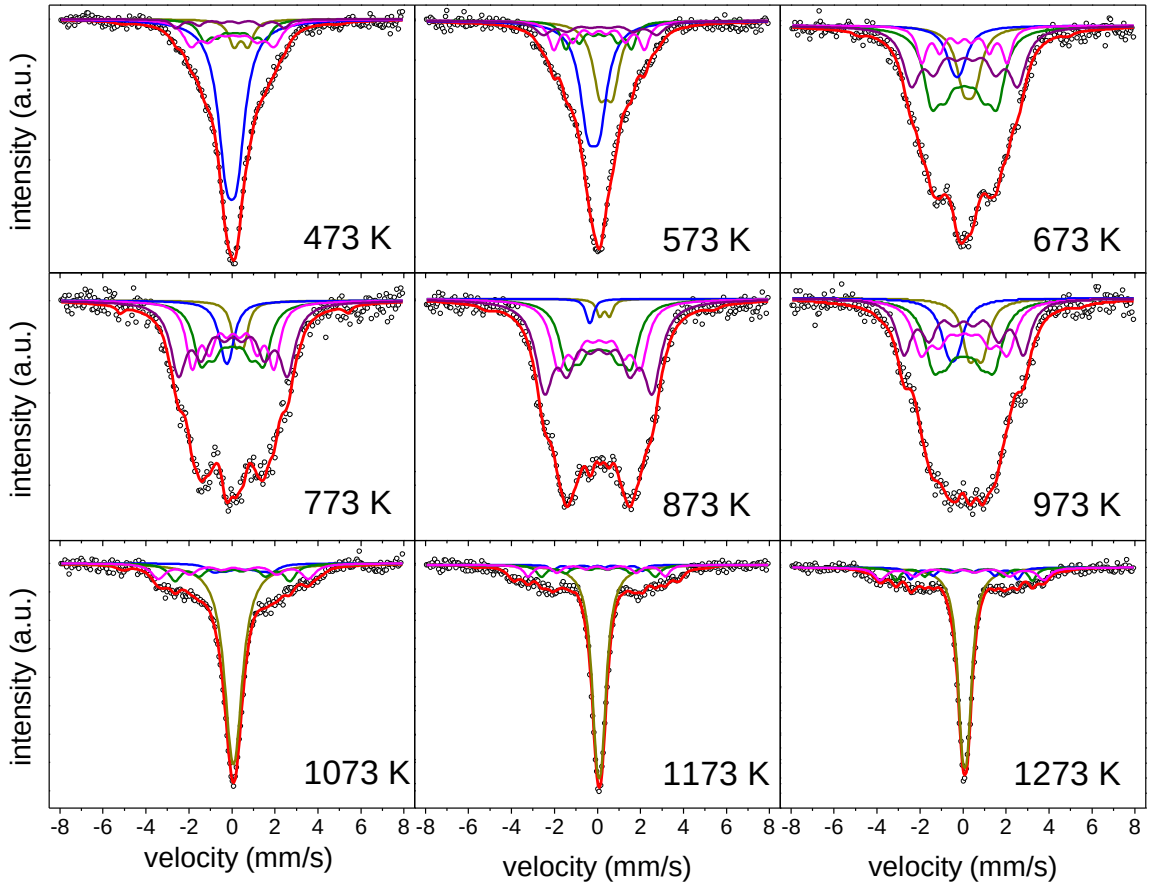

Figure 8. Room temperature Mössbauer spectra of $Ni_{55}Fe_{19}Ga_{26}$ powder sample annealed for 10 min at the marked temperatures

Table 4. Hyperfine parameters at the room temperature of powders samples after annealing at the marked temperatures (T_{ann}). B_{hf} is the magnetic hyperfine field, <B_{hf}> the mean hyperfine field, δ the isomer shift relative to α-Fe, A the Fe atomic fraction, Q the quadruple splitting, and Γ the linewidth of each contribution.

T_{ann} (K)	Component	Q (mm/s)	B_{hf} (T)	<B_{hf}> (T)	δ (mm/s)	Γ (mm/s)	A (%)
1273	Doublet	0.26	-	-	0.084	0.54	63
	Site1	-	15.4	20.2	0.053	0.43	10
	Site 2	-	19.6		0.056	0.46	11
	Site 3	-	23.6		-0.046	0.67	16
1173	Doublet	0.26	-	-	0.079	0.58	62
	Site1	-	12.9	19.6	0.009	0.35	4
	Site 2	-	16.4		0.046	0.57	11
	Site 3	-	19.8		-0.034	0.50	10
	Site 4	-	23.7		-0.068	0.67	13
1073	Doublet	0.24	-	-	0.071	0.86	60

	Site1	-	8.4	17.1	0.051	0.75	8
	Site 2	-	16.5		0.021	0.70	16
	Site 3	-	21.6		0.067	0.8	16
973	Doublet 1	0.61	-	-	0.600	0.77	11
	Doublet 2	0.40	-	-	-0.490	0.86	9
	Site1	-	8.8	12.6	0.036	0.95	30
	Site 2	-	12.5		0.060	0.94	25
	Site 3	-	17.2		0.021	0.84	25
873	Doublet 1	0.45	-	-	0.34	0.45	2
	Doublet 2	0.14	-	-	-0.36	0.35	2
	Site 1	-	9.2	12.8	0.07	0.87	25
	Site 2	-	11.8		0.08	0.83	27
	Site 3	-	15.5		0.05	0.98	44
773	Doublet 1	0.38	-	-	0.36	0.51	6
	Doublet 2	0.22	-	-	-0.23	0.71	7
	Site 1	-	9.0	12.6	0.01	0.81	25
	Site 2	-	11.8		0.06	0.67	25
	Site 3	-	15.7		0.05	0.90	36
673	Doublet 1	0.48	-	-	0.27	0.85	13
	Doublet 2	0.33	-	-	-0.28	0.89	8
	Site 1	-	9.4	12.2	0.06	0.89	35
	Site 2	-	12.3		0.07	0.53	12
	Site 3	-	15.3		0.07	0.96	31
573	Doublet 1	0.58	-	-	0.40	0.80	24
	Doublet 2	0.50	-	-	-0.18	0.91	38
	Site 1	-	9.5	12.7	0.06	0.52	13
	Site 2	-	13.0		0.08	0.55	15
	Site 3	-	16.4		0.12	0.84	11
473	Doublet 1	0.65	-	-	0.42	0.58	7
	Doublet 2	0.50	-	-	-0.01	0.95	55
	Site 1	-	8.8	11.4	0.14	0.65	12
	Site 2	-	12.0		0.03	0.84	20
	Site 3	-	15.5		-0.08	0.51	5

Taking into account the crystal structure of the stoichiometric austenite Ni_2FeGa, the Mössbauer results should give only a FM site corresponding to the Fe atoms in the Y sites (4a) since Fe has only one crystallographic equivalent lattice site (see table 5). The existence of additional components suggests the occurrence of structural disorder. This structural disorder can be due to two main sources; off-stoichiometry effects and the stress induced during mechanical treatment. In this sense, the existence of additional FM sites could be due to the occupation of the Fe atoms of Ni(X) and Ga(Z) sites of the

$L2_1$ phase leading to a disordered structure, typical of samples produced by rapid quenching [10, 13].

Table 5. Near neighbors (NN) in the first two coordination spheres of the three crystallographic sites in a stoichiometric Ni_2FeGa with a $L2_1$ structure.

Site	NN First sphere	NN Second sphere
Ni(X)	4 Fe, 4 Ga	6 Ni
Fe(Y)	8 Ni	6 Ga
Ga(Z)	8 Ni	6 Fe

In order to facilitate the assigning of various B_{hf} components to specific crystallographic sites of the austenite or the gamma phases, temperature dependence of magnetization curves $M(T)$ during cooling and heating at 0.01 T for annealed powder samples have been analyzed. These curves are shown in Figure 9. $M(T)$ shows, with cooling, that samples annealed up to temperatures below 673 K undergo a unique magnetic transition from PM to FM phase in the explored temperature range. Taking into account the XRD results of the powder samples (Figure 7), this transition should correspond to the magnetic transformation of the NM martensite structure, at T_C^M. This temperature increases from 335 to 354 K for the as-milled and the sample annealed at 573 K samples, respectively (see inset of Figure 9).

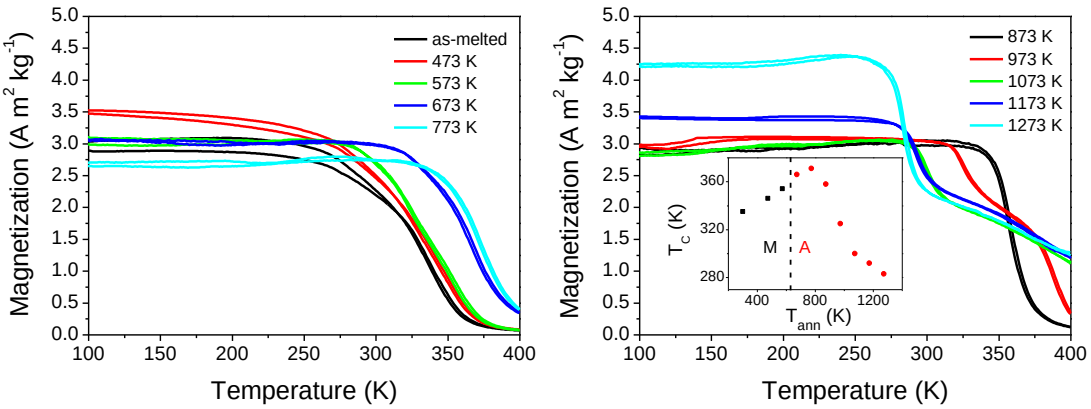

Figure 9. $M(T)$ curves measured upon cooling and heating at 0.01 T for $Ni_{55}Fe_{19}Ga_{26}$ powders after annealing at the marked temperatures. Inset shows the evolution of the Curie temperature of the martensite (M) and the austenite (A) phases with the annealing temperature.

$M(T)$ curves of samples annealed between 673 and 873 K also exhibit a unique transition from PM to FM phase. However, in these cases, it corresponds to the Curie transition of the austenite structure, T_C^A, which are slightly higher than T_C^M for these samples. Finally, $M(T)$ curves of samples annealed above 873 K show two magnetic transitions, corresponding to the austenite and gamma phases. In fact, the presence of the γ-phase, the amount of which monotonically increases with increasing the annealing temperature, is responsible for a non-zero magnetization above T_C^A. These results are in agreement with those reported by Rama Rao *et al.* [13] and Okumura *et al.* [12], who also found that the gamma phase exhibits a Curie transition at higher temperature than the austenite phase. The presence of this γ-phase after annealing is a difference between the Ni-Fe-Ga alloy studied here and Ni-Mn-Ga alloy studied in Ref. [22]. This fact could be the reason why recovery of the modulated phase is not achieved in the former system unlike the latter one.

The decrease of T_C^A with the annealing temperature leads to the austenite phase to become paramagnetic at room temperature. This allows us to assign the FM sites detected by Mössbauer to the γ phase, the unique FM phase at room temperature (see

Table 5). A gradual change of the different contributions used in the fitting as well as an increase in the mean hyperfine field, $<B_{hf}>$ can be observed as the annealing temperature increases. It suggests a continuous structural modification affecting the room temperature structure during the heat treatments. In fact, it has been reported a decrease of the T_C^A with the decrease of Fe content in NiFeGa alloys (at fixed Ga content) [29, 30], that could explain the behavior of the $M(T)$ curves. The increase of the $<B_{hf}>$ at the room temperature is in agreement with the increase of the magnetization observed in the Figure 9.

Only Curie transitions have been observed in the $M(T)$ curves. First order martensitic transformation from FM austenite to PM martensite (on cooling) with a characteristic thermal hysteresis is not observed in none of the studied samples. This supports the DSC results, showing the disappearance of the martensitic transformation with the mechanical treatments, that it is not recovered despite the thermal treatments.

4. CONCLUSIONS

Nickel-rich polycrystalline $Ni_{55}Fe_{19}Ga_{26}$ alloy was prepared in a ribbon shape by melt-spinning. It has been found that the as-spun ribbon exhibits a martensite modulated 14M structure at the room temperature and a martensitic transition at roughly 395 K.

After the ribbon is mechanically treated, the modulated structure changes to a non-modulated structure, thermodynamically more stable. In fact, due to the pulverization of the ribbon, the martensite transition almost vanishes, suggesting that this transition only occurs between the modulated and the $L2_1$ austenite structure. The gradual decrease of the intensity of the DSC peak allows us to estimate the fraction of 14M phase as a function of pressure.

From a series of annealing experiments, it was shown that the original 14M structure cannot be recovered once the ribbon is pulverized, at least, in the range of temperatures and times conducted here. The formation of gamma phase (annealing above 673 K) can be an obstacle to this recovery. It has been found that the annealing stabilizes the austenite structure at room temperature for samples treated at temperatures above 673 K.

The combination of the Mössbauer spectroscopy, X-ray diffraction and magnetization measurements supplies detailed information about the structural changes, the presence of disordering and the magnetic properties of the different phases observed.

Acknowledgements

This work was supported by AEI/FEDER-UE (Project MAT 2016-77265-R and Project US-1260179) and the PAI of the Regional Government of Andalucía. Support of the project APVV-19-0369 is also acknowledged. A.F. Manchón-Gordón acknowledges a VPPI-US fellowship.

References

[1] Chernenko VA, Cesari E, Kokorin VV, Vitenko IN. The development of new ferromagnetic shape-memory alloys in ni-mn-ga system. Scripta Metallurgica Et Materialia 1995;33:1239-44. https://doi.org/10.1016/0956-716X(95)00370-B

[2] Ullakko K, Huang JK, Kantner C, Ohandley RC, Kokorin VV. Large magnetic-field-induced strains in Ni2MnGa single crystals. Applied Physics Letters 1996;69:1966-8. https://doi.org/10.1063/1.117637

[3] Planes A, Manosa L, Acet M. Magnetocaloric effect and its relation to shape-memory properties in ferromagnetic Heusler alloys. Journal of Physics-Condensed Matter 2009;21: 233201. https://doi.org/10.1088/0953-8984/21/23/233201

[4] Liu J, Scheerbaum N, Kauffmann-Weiss S, Gutfleisch O. NiMn-Based Alloys and Composites for Magnetically Controlled Dampers and Actuators. Advanced Engineering Materials 2012;14:653-67. https://doi.org/10.1002/adem.201200038

[5] Sozinov A, Likhachev AA, Lanska N, Ullakko K. Giant magnetic-field-induced strain in NiMnGa seven-layered martensitic phase. Applied Physics Letters 2002;80:1746-8. https://doi.org/10.1063/1.1458075

[6] Pons J, Cesari E, Segui C, Masdeu F, Santamarta R. Ferromagnetic shape memory alloys: Alternatives to Ni-Mn-Ga. Materials Science and Engineering a-Structural Materials Properties Microstructure and Processing 2008;481:57-65. https://doi.org/10.1016/j.msea.2007.02.152

[7] Ducher R, Kainuma R, Ishida K. Phase equilibria in the Ni-Fe-Ga alloy system. Journal of Alloys and Compounds 2008;463:213-9. https://doi.org/10.1016/j.jallcom.2007.09.079

[8] Oikawa K, Omort T, Sutou Y, Morito H, Kainuma R, Ishida K. Phase equilibria and phase transition of the Ni-Fe-Ga ferromagnetic shape memory alloy system. Metallurgical and Materials Transactions a-Physical Metallurgy and Materials Science 2007;38A:767-76. https://doi.org/10.1007/s11661-007-9095-8

[9] Hamilton RF, Sehitoglu H, Efstathiou C, Maier HJ. Inter-martensitic transitions in Ni-Fe-Ga single crystals. Acta Materialia 2007;55:4867-76. https://doi.org/10.1016/j.actamat.2007.05.003

[10] Zhang HR, Wu GH. Atomic-size effect on the microstructural properties of Ni_2FeGa. Acta Materialia 2011;59:1249-58. https://doi.org/10.1016/j.actamat.2010.10.057

[11] Alvarez-Alonso P, Aguilar-Ortiz CO, Villa E, Nespoli A, Flores-Zuniga H, Chernenko VA. Conventional and inverse elastocaloric effect in Ni-Fe-Ga and Ni-Mn-Sn ribbons. Scripta Materialia 2017;128:36-40. https://doi.org/10.1016/j.scriptamat.2016.09.033

[12] Okumura H, Uemura K. Influence of quenching rate on the magnetic and martensitic properties of Ni-Fe-Ga melt-spun ribbons. Journal of Applied Physics 2010;108:043910

[13] Rama Rao NV, Gopalan R, Manivel Raja M, Chandrasekaran V, Suresh KG. Mossbauer studies on structural ordering and magnetic properties of melt-spun Ni-Fe-Ga ribbons. Applied Physics Letters 2008;93:202503. https://doi.org/10.1063/1.3465613

[14] Villa E, Aguilar-Ortiz CO, Nespoli A, Alvarez-Alonso P, Camarillo-Garcia JP, Salazar D, et al. Tailoring thermomechanical treatment of Ni-Fe-Ga melt-spun ribbons for elastocaloric applications. Journal of Materials Research and Technology-Jmr&T 2019;8:4540-6. https://doi.org/10.1016/j.jmrt.2019.07.067

[15] Liu J, Scheerbaum N, Hinz D, Gutfleisch O. Martensitic transformation and magnetic properties in Ni-Fe-Ga-Co magnetic shape memory alloys. Acta Materialia 2008;56:3177-86. https://doi.org/10.1016/j.actamat.2008.03.008

[16] Lopez-Garcia J, Unzueta I, Sanchez-Alarcos V, Recarte V, Perez-Landazabal JI, Rodriguez-Velamazan JA, et al. Correlation between defects and magneto-structural properties in Ni-Mn-Sn metamagnetic shape memory alloys. Intermetallics 2018;94:133-7. https://doi.org/10.1016/j.intermet.2017.12.028

[17] Tian B, Chen F, Liu Y, Zheng YF. Effect of ball milling and post-annealing on magnetic properties of $Ni_{49.8}Mn_{28.5}Ga_{21.7}$ alloy powders. Intermetallics 2008;16:1279-84. https://doi.org/10.1016/j.intermet.2008.08.002

[18] Tian B, Chen F, Liu Y, Zheng YF. Structural transition and atomic ordering of Ni49.8Mn28.5Ga21.7 ferromagnetic shape memory alloy powders prepared by ball milling. Materials Letters 2008;62:2851-4. https://doi.org/10.1016/j.matlet.2008.01.071
[19] Gutierrez J, Lazpita P, Barandiaran JM, Garitaonandia JS, Plazaola F, Legarra E, et al. Mössbauer study of the martensitic transformation in a Ni-Fe-Ga shape memory alloy. Hyperfine Interactions 2006;168:1207-10. https://doi.org/10.1007/978-3-540-49853-7_83
[20] Barandiaran JM, Gutierrez J, Lazpita P, Chernenko VA, Segui C, Pons J, et al. Martensitic transformation in Ni-Fe-Ga alloys. Materials Science and Engineering a-Structural Materials Properties Microstructure and Processing 2008;478:125-9. https://doi.org/10.1016/j.msea.2007.05.097
[21] Tolea F, Sofronie M, Crisan AD, Enculescu M, Kuncser V, Valeanu M. Effect of thermal treatments on the structural and magnetic transitions in melt-spun Ni-Fe-Ga-(Co) ribbons. Journal of Alloys and Compounds 2015;650:664-70. https://doi.org/10.1016/j.jallcom.2015.07.296
[22] Chernenko VA, Pons J, Cesari E, Ishikawa K. Stress-temperature phase diagram of a ferromagnetic Ni-Mn-Ga shape memory alloy. Acta Materialia 2005;53:5071-7. https://doi.org/10.1016/j.actamat.2005.07.018
[23] Gaitzsch U, Potschke M, Roth S, Mattern N, Rellinghaus B, Schultz L. Structure formation in martensitic $Ni_{50}Mn_{30}Ga_{20}$ MSM alloy. Journal of Alloys and Compounds 2007;443:99-104. https://doi.org/10.1016/j.jallcom.2006.10.011
[24] Zayak AT, Entel P. Role of shuffles and atomic disorder in Ni-Mn-Ga. Materials Science and Engineering a-Structural Materials Properties Microstructure and Processing 2004;378:419-23. https://doi.org/10.1016/j.msea.2003.10.368
[25] Manchon-Gordon AF, Ipus JJ, Blazquez JS, Conde CF, Conde A. Evolution of Fe environments and phase composition during mechanical amorphization of $Fe_{70}Zr_{30}$ and $Fe_{70}Nb_{30}$ alloys. Journal of Non-Crystalline Solids 2018;494:78-85. https://doi.org/10.1016/j.jnoncrysol.2018.04.061
[26] Pizarro R, Garitaonandia JS, Plazaola F, Barandiaran JM, Greneche JM. Magnetic and Mossbauer study of multiphase Fe-Zr amorphous powders obtained by high energy ball milling. Journal of Physics-Condensed Matter 2000;12:3101-12. https://doi.org/10.1088/0953-8984/12/13/318
[27] Manchon-Gordon AF, Moreno-Ramirez LM, Ipus JJ, Blazquez JS, Conde CF, Franco V, et al. A procedure to obtain the parameters of Curie temperature distribution from thermomagnetic and magnetocaloric data. Journal of Non-Crystalline Solids 2019;520:119460. https://doi.org/10.1016/j.jnoncrysol.2019.119460
[28] Oikawa K, Ota T, Ohmori T, Tanaka Y, Morito H, Fujita A, et al. Magnetic and martensitic phase transitions in ferromagnetic Ni-Ga-Fe shape memory alloys. Applied Physics Letters 2002;81:5201-3. https://doi.org/10.1063/1.1532105
[29] Barandiaran JM, Chernenko VA, Lazpita P, Gutierrez J, Feuchtwanger J. Effect of martensitic transformation and magnetic field on transport properties of Ni-Mn-Ga and Ni-Fe-Ga Heusler alloys. Physical Review B 2009;80:104404. https://doi.org/10.1103/PhysRevB.80.104404
[30] Pal D, Mandal K. Magnetocaloric effect and magnetoresistance of Ni-Fe-Ga alloys. Journal of Physics D-Applied Physics 2010;43:455002. https://doi.org/10.1088/0022-3727/43/45/455002